Phase Structures in the Micromaser Photon Statistics*

János A. Bergou and Pál Bogár

Department of Physics and Astronomy, Hunter College of the City University of New York, 695 Park Avenue, New York, New York 10021, USA

Z. Naturforsch. **54 a,** 39–49 (1999); received September 24, 1998

In the photon number distribution $p(\theta, k)$ of the micromaser, distinct structures are formed by the ridges connecting the peaks in the $\theta - k$ space. We refer to these structures as phases. By a simple condition we can distinguish between "semiclassical" and "quantum" regimes of operation near and far above threshold, respectively. In the semiclassical regime, the equations of state of the phases $\theta = \theta(k)$ are monotonous and coincide with the steady state solutions of the semiclassical theory. They reflect typical features of the micromaser dynamics. The transition jumps, e. g., between the phases decrease with increasing pumping parameter θ, signifying the onset of the Jaynes-Cummings collapse. On increasing θ further, the phases first disintegrate and then restructure into new kinds of phases in the quantum regime. The equations of state are no longer monotonous. Large single peaks, the quantum island states (QIS), develop in the neighborhoods of minima. The system undergoes oscillations between two kinds of quantum island states, QIS^- and QIS^+, as a function of θ. The disintegration and transformation of phases recur periodically as θ is varied, and the phases in the semiclassical region are followed by consecutive phase structures in the quantum regime. The subsequent collapses and revivals of phases are directly connected to the Jaynes-Cummings collapse and revival. The observation of these phase structures and the accompanying QIS is experimentally feasible.

PACS 42.50.Dv, 42.52+x

1. Introduction

One of the most extensively studied systems in quantum optics is the so-called micromaser, or one-atom maser [1]. It realizes the fundamental Jaynes-Cummings model [2] by coupling a single quantized mode of a high-Q microwave cavity to a sparse beam of two-level atoms. Due to the relatively straightforward theory [3, 4] and experimental accessibility, it has proved to be particularly well suited to study quantum effects in the interaction between radiation and matter. Genuine quantum features have been predicted and observed, such as, e. g, the Jaynes-Cummings collapse-revival [5], nonclassical photon statistics including number states [6], trapping states [7], quantum island states [8], and macroscopical superpositions [9]. It has also been suggested to build macroscopic correlated systems by coupling two micromasers together to study nonlocal quantum correlations between separate fields [10], or to couple them to other quantum devices in, for example, atomic interferometers to test the principle of complementarity [11].

In the present paper we study the photon statistics of a micromaser pumped by a monoenergetic beam of two-level atoms with Poissonian arrival statistics. It is shown that the photon distribution consists of distinct phases. We study their structure in the two-dimensional space given by the pump parameter θ and the photon number k. A correspondence between the quantum [3] and semiclassical [4] theories of the problem will be pointed out and used to find the equation of state of the phases. The photon statistics of the system can be separated into "semiclassical" and "quantum" regimes with very different behaviors due to the crucial role of the quantized nature of the field in the latter regime. We show that this picture of phase structures in the photon statistics can explain several features of the micromaser both qualitatively and quantitatively.

In Sect. 2 and 3 we investigate the semiclassical and quantum regimes of the system, respectively. Section 4 is devoted to summary and discussions, while

* Dedicated to Professor Süßmann on occasion of his 70th birthday.

Reprint requests to Prof. J. Bergou; Fax: +1 212 772 5390, E-mail: jbergou@shiva.hunter.cuny.edu.

0932–0784 / 99 / 0100–0039 $ 06.00

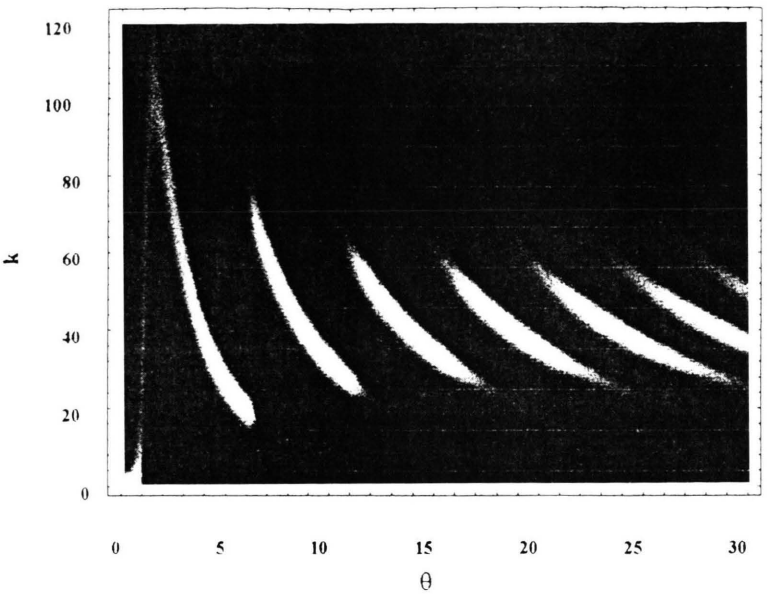

Fig. 1. Density plot of the photon statistics in the semiclassical regime for $N_{\rm ex} = 100$ and $\overline{n}_b = 0.5$. Lighter points in the figure show higher probabilities. Bright ridges form a phase structure of the system.

in the Appendix we derive some of the necessary formulas used in the paper.

2. The Semiclassical Regime

Let us consider a micromaser [1] where a single quantized mode of a high-Q microwave cavity is pumped by a monoenergetic beam of excited two-level atoms. Assuming that there is at most one atom present in the cavity at a time and that the interaction time, τ, is much shorter than the cavity lifetime, $1/\gamma$, the photon statistics can be calculated as [3]

$$p_n(\theta) = p_0(\theta) \prod_{k=1}^{n} E(k,\theta), \tag{2.1}$$

where

$$E(k,\theta) = \frac{N_{\rm ex}}{k(\overline{n}_b + 1)} \beta(k,\theta) + \frac{\overline{n}_b}{\overline{n}_b + 1} \tag{2.2}$$

and

$$\beta(k,\theta) = \sin^2\left(\theta\sqrt{k/N_{\rm ex}}\right). \tag{2.3}$$

Here, the average number of atoms inside the cavity during the cavity lifetime is given by $N_{\rm ex} = r/\gamma$, where r is the average rate of injection of the atoms, and the pumping parameter is defined by $\theta = g\tau\sqrt{N_{\rm ex}}$ where g is the atom-field coupling constant. Finite thermal radiation is also assumed, specified by the average number of thermal photons $\overline{n}_b$.

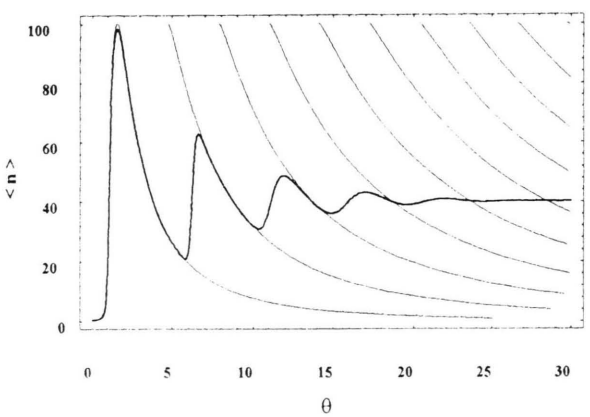

Fig. 2. Stable and unstable solutions of the semiclassical theory depicted by light solid and dotted lines, respectively. The stable solutions correspond to the bright ridges in Figure 1. The average photon number $\langle n \rangle$, calculated from the photon statistics of Fig. 1 is represented by a heavy solid line showing the transitions that the system makes between the phases as a function of the pumping parameter θ.

Figure 1 indicates that the above photon statistics specifies an ensemble of phases in the θ-k space where small changes in the pumping parameter θ result in small changes in the photon number k. The smooth evolution along the phases is periodically interrupted by abrupt transitions between them at certain critical values of θ. Their structure is clearly reminiscent

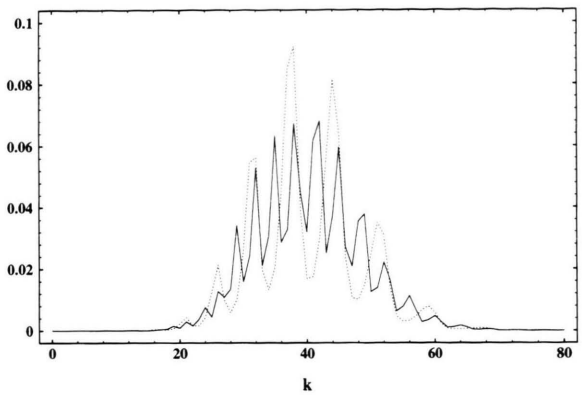

Fig. 3. Photon statistics for $\theta = 60$ and 120 depicted by dotted and solid lines, respectively. The envelope of the peaks is a bell-shaped curve that is fairly independent of θ.

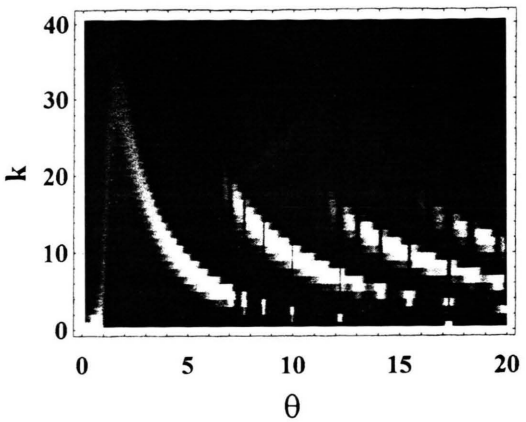

Fig. 4. Density plot of the photon statistics for $N_{\rm ex} = 30$ and $\overline{n}_b = 0$. The distinct bright spots are the probability peaks of the trapping states. The dark lines parallel to the k-axis above the peaks indicate how the probability distribution is blocked and the system is forced back to a lower order phase in this case.

of the (multi-) stable steady states of the semiclassical theory [4], illustrating the connection between the quantum and the semiclassical approach (cf. Figs. 1 and 2). Employing the stable (unstable) solutions for the semiclassical steady states, this correspondence can be used to determine the location of the peaks (minima) and the equation of state for the phases of the photon statistics. It is, however, unique to the quantum theory to provide a probability distribution and to account for the effects originating in the shape of the photon statistics. This is beyond the grasp of the semiclassical approach. Let us now review some of these quantum effects. It can be seen in Figs. 1, 6 and 7 that, apart from some exceptional cases, the photon statistics is confined to a narrow region of the photon number k, centered around approximately 40% of $N_{\rm ex}$. The envelope of the peaks is a bell-like curve (see Fig. 3) that is fairly independent of θ. Multipeaked photon statistics arise when the phases populated in this region of k overlap at a given pump parameter θ. This overlap forces the system to switch from one phase to the next via a first order phase transition accompanied by a sudden increase in the photon number noise [1, 3, 4, 8]. Figure 2 illustrates how the quantum treatment results in a suppression of the multistable behavior. The average photon number becomes single-valued as it selects between the available branches of the semiclassical theory according to the probability distribution of the quantum theory. It can be seen, however, that the phase transitions decay to a θ-independent constant value as the number of overlapping phases increases. This occurs because, due to the increasing number of the peaks under the bell-curve, the average photon number becomes less sensitive to the appearances of new peaks. This effect is directly related to the Jaynes-Cummings collapse [5] since the atomic inversion, w, is a simple function of the average photon number $\langle n \rangle$ given by $w = 1 - 2(\langle n \rangle - \overline{n}_b)/N_{\rm ex}$ (see derivation in the Appendix). In the case of no thermal radiation $\overline{n}_b = 0$, the trapping states play a role [7]. They significantly modify the phase structure by trapping the system in a lower order phase in certain narrow regions of the pumping parameter θ (see Figure 4).

As we mentioned above, we can make use of the correspondence between the quantum and semiclassical theories to find the equation of the phases. The semiclassical steady states are determined by the equation (see [4] and an alternative derivation in the Appendix)

$$\theta\sqrt{(k_0+1)/N_{\rm ex}} = \mp \mathrm{Arcsin}\left(\sqrt{(k_0-\overline{n}_b)/N_{\rm ex}}\right) + l\pi, \tag{2.4}$$

where the minus (plus) sign corresponds to the stable (unstable) solutions depicted by solid (dotted) lines in Fig. 2, while $l = 0, 1, 2, \ldots$ enumerates them. It can be seen by comparing Figs. 1 and 2 that the peaks (minima) of the photon statistics coincide with the stable (unstable) solutions. Equation (2.4) can be simplified if we assume a small number of thermal photons,

$\overline{n}_b \approx 1$, and also $1 \ll k_0 \ll N_{ex}$. This latter assumption simply accounts for the photon statistics being confined to a narrow region of the photon number around 0.4 N_{ex}. This way, the first term on the right hand side of (2.4) can be reduced to $\mp\sqrt{k_0/N_{ex}}$. On the left hand side we can neglect the +1 provided

$$\theta\sqrt{(k_0+1)/N_{ex}} - \theta\sqrt{k_0/N_{ex}} \ll 1 \qquad (2.5)$$

in a vicinity of k_0. This difference can be approximated with $\theta\sqrt{4k_0N_{ex}}$ for $k_0 \ll 1$, yielding the following condition for the pumping parameter:

$$\theta \ll \sqrt{k_0 N_{ex}}. \qquad (2.6)$$

In this region of the parameters the quantized nature of the field does not play a significant role and, therefore, we call it the "semiclassical" regime of the micromaser. Since there cannot be peaks for $k_0 > N_{ex}$ [8], this condition tells us in short that θ cannot be larger than N_{ex} in this regime. Using these approximations, (2.4) reduces to the simple expression

$$k_{0\pm} = N_{ex}\left(\frac{l\pi}{\theta \pm 1}\right)^2, \qquad (2.7)$$

determining the location of the peaks and minima of the photon statistics $k_{0\pm}$ for a given θ in the semiclassical regime taking the plus and minus signs, respectively. The system exhibits a structure consisting of continuous and smooth phases here, as depicted in Figs. 1, 2 and 6. However, as we will show later on, these phases will be disintegrated and reshaped at high pumping parameters beyond the region of (2.6) where the discreteness of the photon number becomes significant.

The same result can be obtained by using the function $E(k,\theta)$ from the quantum solution, as given by (2.2). One finds a peak (minimum) of the photon statistics at a photon number, k_0, if $E(k_0,\theta) > 1$ (< 1) and $E(k_0+1,\theta) < 1$ (> 1). In the case when the change in the function $E(k,\theta)$, produced by one discrete step of the photon number from k_0 to k_0+1, is small, the quantum nature of the radiation field is not significant and these two conditions can be approximated in a neighborhood of $k_0 \gg 1$ by

$$E(k_0,\theta) = 1 \text{ and } \pm\left(\frac{\partial E}{\partial k}\right)(k_0,\theta) > 0. \qquad (2.8)$$

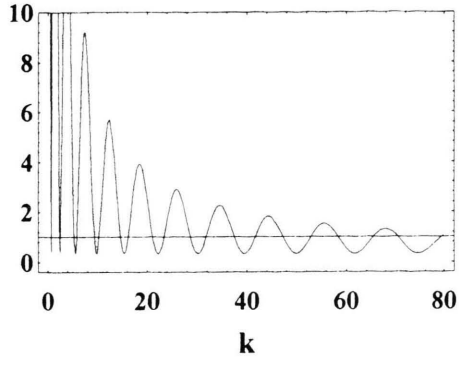

Fig. 5. The function $E(k,\theta)$ and its discrete counterpart $E_k(\theta)$, depicted by solid and dashed lines, respectively, for $\theta = 40$, $N_{ex} = 100$ and $\overline{n}_b = 0.5$. For these parameters the two functions agree rather well. The agreement will disappear for larger θ.

Here the upper (lower) sign corres ponds to a peak (minimum). In order to specify the region where these conditions are valid and to visualize the effect of the quantized photon number let us define the discrete counterpart, $E_k(\theta)$, of the continuous function $E(k,\theta)$, as the curve connecting the discrete points $(k, E(k,\theta))$ taken at integer values of k, by straight lines. The continuous function $E(k,\theta)$ oscillates faster for larger θ (and smaller k), suggesting that $E_k(\theta)$ will deviate from it high above threshold (and at small photon numbers). We find that $E_k(\theta)$ follows $E(k,\theta)$slowly with k in a neighborhood of k_0, i. e., if the conditions given by (2.5) and (2.6) for $k_0 \gg 1$ apply. In this region of the parameters, i. e., in the semiclassical regime, $E_k(\theta)$ can be approximated by the continuous function $E(k,\theta)$, and (2.8) can be used. An example for this case is depicted in Fig. 5, while the deviation between the two functions is apparent in Figs. 9 and 10 that will be discussed later on in detail. One can see in Fig. 5 that $E(k,\theta)$ is an oscillatory function and its minima are given by the curves

$$\theta_{min}^2 k_{min} = (l\pi)^2 N_{ex}, \qquad (2.9)$$

in the θ-k space, where l is an integer. Expanding $E(k,\theta)$ with respect to θ for a given k_0 around one of the minima θ_{min}, we find that $E \leq 1$ if $\theta_{min} - 1 \leq \theta \leq \theta_{min} + 1$, provided $k_0 \ll N_{ex}$. The derivative of $E(k,\theta)$ with respect to k in the vicinity of $k_0 \gg 1$ at the lower (upper) end of this interval is negative (positive). Thus, considering the above conditions for

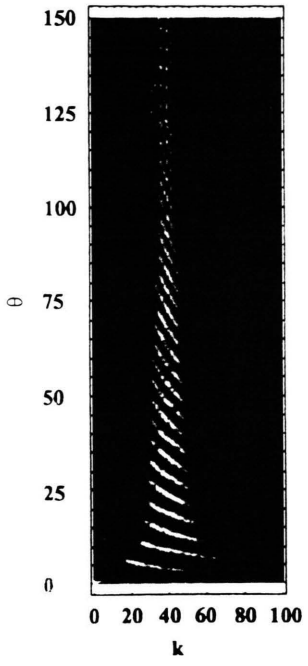

Fig. 6. Density plot of the photon statistics for $N_{\rm ex}$ = 100 and $\overline{n}_b$ = 0.5. The bright ridges of the semiclassical regime become diffuse for large θ as the system approaches the quantum regime. They disintegrate because, due to the increased slope of the phases, the discreteness of the photon number becomes more significant.

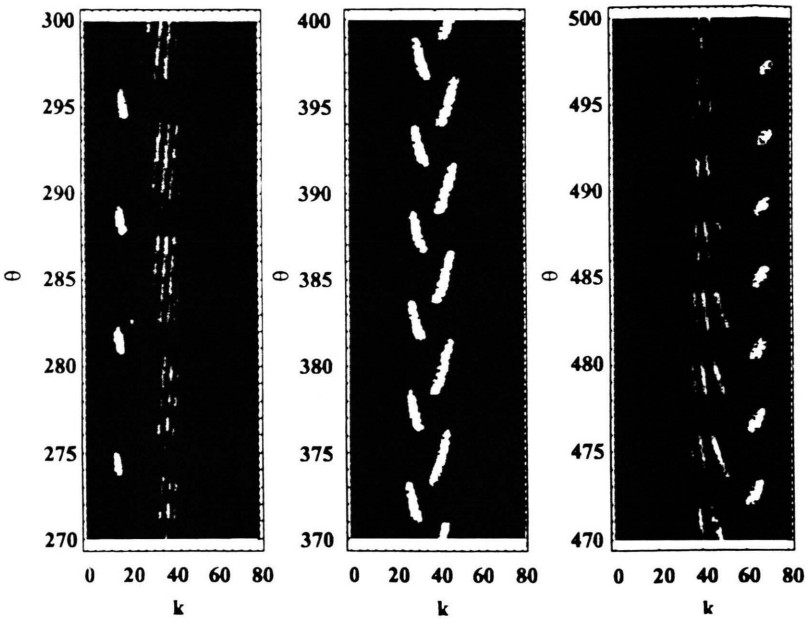

Fig. 7. Density plots of three regions of the photon statistics in the quantum regime of s = 1 for $N_{\rm ex}$ = 100 and $\overline{n}_b$ = 0.5. Bright ridges and well localized spots are apparent, showing the phase structure and the accompanying quantum island states of the system, respectively .

peaks (minima) of the photon statistics (2.8), we find for $1 \ll k_0 \ll N_{\rm ex}$ that they are located on curves shifted downward (upward) by 1 with respect to the curves of the minima of the function $E(k, \theta)$. Carrying out this shifting in (2.9), we reobtain the same result as in (2.7). It determines the location of the peaks and the minima of the photon statistics in the so-called semiclassical regime of the micromaser specified by the condition (2.6).

3. The Quantum Regime

It can be seen in Fig. 6 that the photon statistics become diffuse as one increases the pumping parameter θ beyond the semiclassical regime. The reason for this is that the granular feature of the phases originating in the discreteness of the photon number becomes significant as a result of their increased slope. Namely, the branches of the stable steady state solutions of the semiclassical theory get closer to each other than one quantum of the photon number, resulting in a disintegration of the phases of the photon statistics. Based on the dominant role of the quantized nature of the radiation field we call this region of the parameters where (2.6) does not apply the "quantum regime" of the micromaser. However, as it can be seen in Fig. 7 the fragments of the disintegrated phases of the semiclassical regime form new structures at larger pumping parameters. The diffuse region is followed by an ensemble of new kinds of apparently smooth phases accompanied by sharp single peaks, the so-called "quantum islands" [8]. The formation of the new phases can be understood as another way to connect the location of the nonzero probabilities of the disintegrated phases

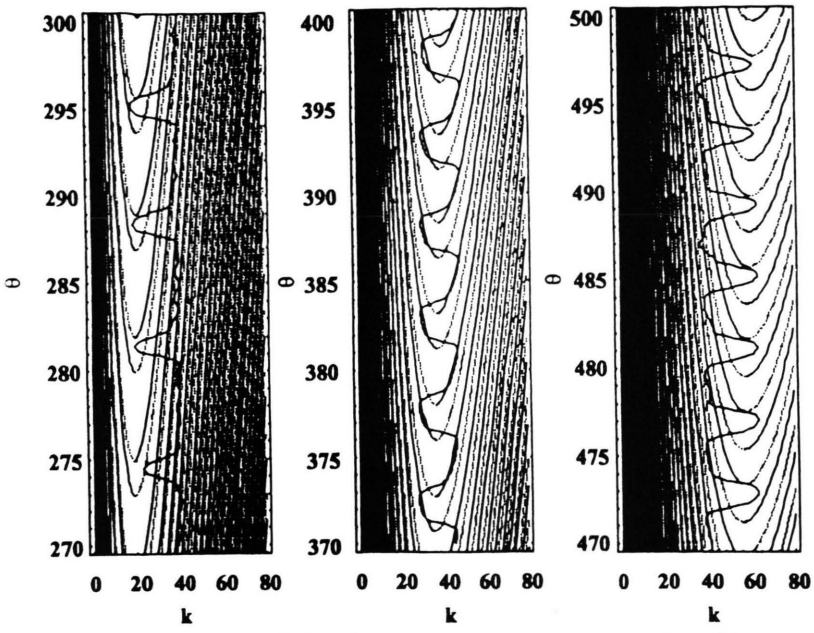

Fig. 8. Phase structure given by (3.1), where the phases and the minima are depicted by light solid and dotted lines, respectively. The light solid lines correspond to the bright ridges in Figure 7. The average photon number, $\langle n \rangle$, calculated from the photon statistics of Fig. 7 is represented by a heavy solid line. The phase transitions of the system between the quantum islands as a function of θ are clearly visible in the middle figure.

on the discrete lattice of the photon number. These new connection rules can be determined by introducing a new parametrization of the phases. Since there are several ways to connect the probability points, therefore, there are several possible connection rules and phase parameters that can be introduced. Let us define a new parameter L as $L = l - sk_0$, where k_0 is the photon number, $s = 0, 1, 2,...$ parametrizes the different connection rules and L is integer. The l parameter of the semiclassical regime can be reobtained for $s = 0$, while several new ones are given by $s > 0$. Substituting the new l into (2.4) we obtain

$$\theta\sqrt{(k_0+1)/N_{\rm ex}} = \mp \mathrm{Arcsin}\left(\sqrt{(k_0-\overline{n}_b)/N_{\rm ex}}\right) + (L+sk_0)\pi. \quad (3.1)$$

Since the disintegration of the old phases and the formation of the new ones is a direct consequence of the quantized nature of the radiation field, (3.1) has nothing to do with the semiclassical theory unless $s = 0$. However, it can now be used to find the location of the peaks (minima) of the photon statistics in the quantum regime the same way as we used (2.4) before for the semiclassical region. The correspondence between (3.1) and the quantum phases is apparent in the examples depicted in Figs. 7 and 8 for $s = 1$. The solid (dotted) lines in Fig. 8 coincide with the peaks (minima) of the photon statistics in Figure 7. The curves with a solid branch on their lower (higher) photon number sides correspond to the upper (lower) sign in (3.1). The average photon number is depicted by a thick solid line in Figure 8. The disintegration of the phases of the semiclassical regime, $s = 0$, led to the formation of the $s = 1$ quantum phases. This is true in general. A disintegrated phase structure of order s is followed by a set of new phases and quantum islands of order $s + 1$. The single semiclassical regime is followed by several consecutive quantum regions.

It can be seen in Figs. 7 and 8 that the phases in the quantum regime are not monotonous curves in the θ-k space as they were in the semiclassical region. Their minima, i. e. the minima of the equations of state of the phases $\theta = \theta(k)$, are located at

$$k^{\rm min} \cong L/s \text{ and } \theta^{\rm min} \cong 2\pi\sqrt{sLN_{\rm ex}} \mp 1, \quad (3.2)$$

provided $1 \ll k^{\rm min} \ll N_{\rm ex}$. These points are important because, as we will see later on, large single peaks, the quantum islands, can arise in their vicinity due to the small slope of the phases. In order to understand this and to find a compact formula for the peaks (minima) of the photon statistics, we make use of the function $E(k, \theta)$ and its discrete counterpart $E_k(\theta)$, again. These functions are useful in explaining why the two branches of each curve in Figure 8 alternatively represent peaks (solid lines) and minima (dotted lines) of the photon statistics. The equation for the minima of $E(k, \theta)$, in terms of the new parameter L,

can be obtained from (2.9) as

$$\theta_{\min} k_{\min} = [(L + s k_{\min})\,\pi]^2\, N_{\rm ex}. \qquad (3.3)$$

As a consequence of the nonzero s, the curves $\theta = \theta(k)$, describing the minima of the function $E(k, \theta)$, as obtained from (3.3), themselves exhibit minima in the θ-k space at

$$k_{\rm MIN} \cong L/s \text{ and } \theta_{\rm MIN} \cong 2\pi\sqrt{sLN_{\rm ex}}, \qquad (3.4)$$

provided $1 \ll k_{\rm MIN}$. The location of the peaks (minima) of the photon statistics can now be calculated similarly to the semiclassical region by shifting the curves of (3.3) by 1 provided $k_{\rm MIN} \ll N_{\rm ex}$. Thus, we reobtain the results for the extremal points of the phases/minima given by (3.2) above as $k^{\rm min} = k_{\rm MIN}$ and $\theta^{\rm min} = \theta_{\rm MIN} \mp 1$. However, due to the non-monotonous feature of the curves, in this case a shift downward (upward) will give us the peaks (minima) only for photon numbers, $k < k_{\rm MIN}$, while opposite shifts are necessary for $k > k_{\rm MIN}$. This is why the two branches of the curves in Fig. 8 alternatively represent the peaks and minima depicted by solid and dotted lines, respectively. Therefore, the equations of the phases of order s are given by

$$(\theta \pm 1)^2 k_0 = \left[(L + s k_0)\right]^2 N_{\rm ex}, \qquad (3.5)$$

where the upper (lower) sign corresponds to the peaks (minima) of the photon statistics for the lower region of the photon numbers, $k < k_{\rm MIN}$, while for the upper part of the photon numbers, $k > k_{\rm MIN}$, the $\pm$ signs need to be switched to $\mp$. Combining these conditions, we finally obtain for a given θ the location of the peaks along one of the phases of the photon statistics in the quantum regime as

$$k_{0\pm} = \frac{k_{\rm MIN}}{\theta_{\rm MIN}^2}\left[\theta \pm 1 \mp \sqrt{(\theta \pm 1)^2 - \theta_{\rm MIN}^2}\right]^2, \qquad (3.6)$$

where $k_{\rm MIN}$ and $\theta_{\rm MIN}$ determine via s (> 0) and L the actual phase that we are considering (see (3.4) above), and the upper (lower) sign gives us a peak below (above) the minimum $k_{\rm MIN}$ of the actual phase. The expression for the minima of the photon statistics can be obtained by switching the two signs, $\pm \rightarrow \mp$.

It can be seen in Fig. 7 that all the phases in the quantum regime exhibit sharp peaks in the vicinity of the minima of their state equation lines. Suppressing everything else at optimum pumping they are the only significant features of the photon statistics (see Figures 9 - 11). These are the so-called "quantum island states" (QIS) discussed in [8] in detail. It follows from the product form of (2.1) that high peaks in the photon statistics are generated when the oscillations of $E_k(\theta)$, as a function of k, are slow. There are long intervals in this case where $E_k(\theta)$ is steadily smaller (larger) than 1 and, consequently, the probability $p_k(\theta)$ is monotonously decreasing (increasing).

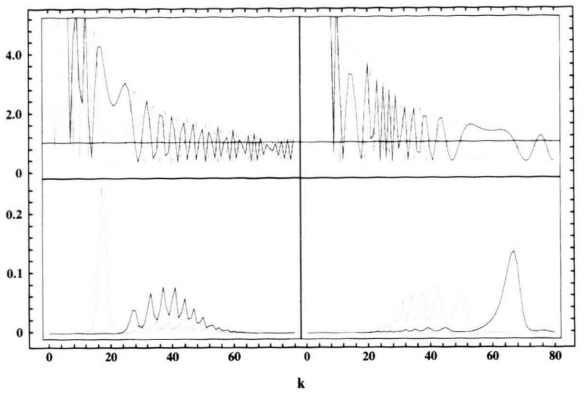

Fig. 9. The functions $E_k(\theta)$ in the upper, and the corresponding photon statistics in the lower part of the figure for four different pumping parameters: θ = 286 and 288, depicted by solid and dotted lines in the left, and θ = 481 and 483, depicted by solid and dotted lines in the right part of the figure, respectively.

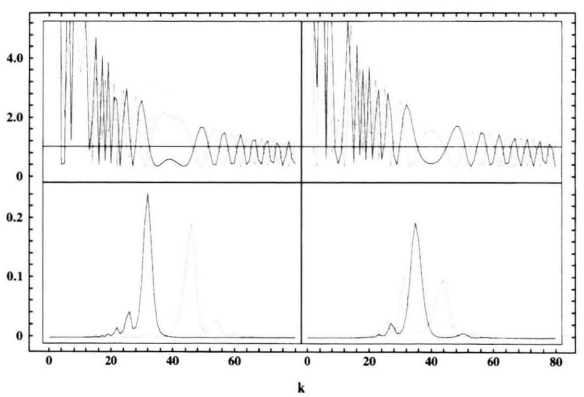

Fig. 10 The functions $E_k(\theta)$ in the upper, and the corresponding photon statistics in the lower part of the figure for four different pumping parameters: θ = 393 and 395, depicted by solid and dotted lines in the left, and θ = 397 and 399, depicted by solid and dotted lines in the right part of the figure, respectively.

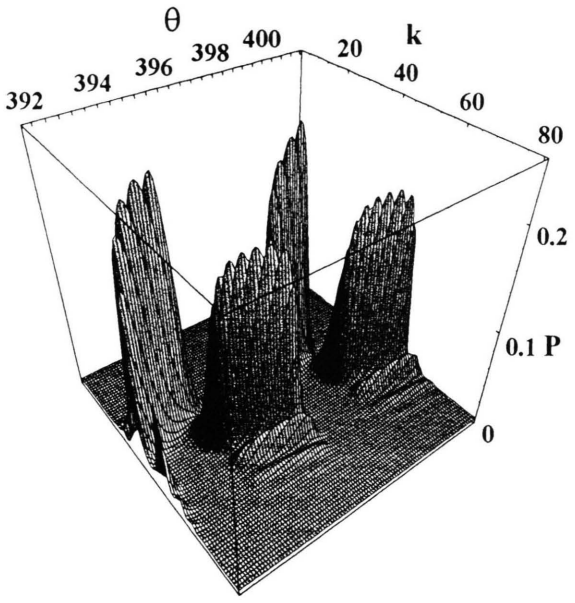

Fig. 11 Three dimensional plot of the photon statistics exhibiting consecutive quantum island states, QIS$^-$ and QIS$^+$.

This, after normalization, will result in a large peak at the beginning (end) of the in terval. One would expect from (2.3) that the oscillations are faster for larger pumping parameter θ, resulting in rapidly oscillating photon statistics. However, this is not so. Although the oscillations of $E(k,\theta)$ are faster, its discrete counterpart $E_k(\theta)$ can deviate from it in the quantum regime as a consequence of the discreteness of the photon number. The oscillations of $E_k(\theta)$ are particularly slow in the neighborhoods of the minima of the phases in the θ-k plane due to the small slope of the phase curves. Some examples are depicted in Figs. 9 and 10 exhibiting long intervals where the $E_k(\theta)$ functions are steadily smaller or larger than 1, resulting in the corresponding QIS shown underneath. The two kinds of slowly varying intervals can be interpreted as two special cases of the Moiré-effect between the oscillations of $E(k,\theta)$ and the discrete periodic lattice of the photon number. Suppressing most of the photon statistics, this effect plays the role of a trapping mechanism making the QIS the "trapping states" in the quantum regime. This trapping effect has obviously nothing to do with the one in [7]. Here, the QIS are the consequence of the quantized nature of the radiation field and the coherent oscillatory nature of the atom-field interaction, reflected by the function $\beta(k,\theta)$ in (2.3). Just as the entire phase structure of the photon statistics, these states, too, are insensitive to (a moderate amount of) thermal radiation.

The two kinds of slowly varying "Moiré-intervals" also suggest that there are two kinds of quantum island states, QIS$^-$ and QIS$^+$, depending whether $E_k(\theta)$ is smaller or larger than 1 in that particular interval, respectively. Therefore, QIS$^-$ (QIS$^+$) are sitting on the low (high) photon number sides of the phase curves, close to their minima (cf. Figs. 7 and 8). Their exact locations can be calculated using (3.6) provided θ is known. However, the optimum pumping, $\theta_{\rm QIS}$, that produces the largest single peaks is, in general, difficult to determine due to the complicated structure of $E_k(\theta)$. Considering Figs. 7 and 8 it can be said that the largest peaks can be produced using a $\theta_{\rm QIS}$ that is equal or slightly smaller than the minimum of a phase curve, $\theta^{\rm min}$. Using $\theta^{\rm min} = \theta_{\rm MIN} \mp 1$, we obtain the optimum pumping to produce QIS as

$$\theta_{\rm QIS^{\pm}} \lessapprox \theta_{\rm MIN} \mp 1. \tag{3.7}$$

where the upper (lower) sign corresponds to QIS$^+$ (QIS$^-$), and $\theta_{\rm MIN}$ is given in (3.4). However, these are only the possible locations of the QIS. Although a long constant interval of $E_k(\theta)$ in the vicinity of the minimum of a phase is necessary for the build-up of a large QIS-peak, it is not, in general, sufficient. As it can be seen in the examples of Fig. 9, QIS$^-$ (QIS$^+$) cannot be generated on the high (low) photon number side of the photon statistics. This is a consequence of the product form of the photon statistics given by (2.1) and the confinement of the photon statistics around 0.4 $N_{\rm ex}$. There is no such problem in Figure 10. Both QIS$^-$ and QIS$^+$ can be produced in that region of the pumping where the minimum of the phases (and the corresponding long interval of constant $E_k(\theta)$) are situated in the main stream of the photon statistics, i. e. around $k = 40$ in our example. Apart from the rapid transitions between them, the micromaser resides in either QIS$^-$, or QIS$^+$ (see Figs. 7 and 8). Therefore, any pumping will result in large single peaks in this region although the optimum cases are still determined by (3.7).

In general, due to the isolated large QIS-peaks, isolated phases become greatly populated in this region of θ at the expense of the others. Similarly to the beginning of the semiclassical regime, there is practically no overlap between the populated parts of these dominant phases that makes the phase transitions abrupt between them. This suggests the interpretation

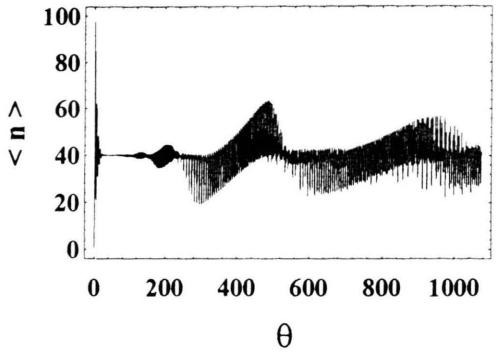

Fig. 12. Average photon number, $\langle n \rangle$, for $N_{ex} = 100$ and $\overline{n}_b = 0.5$, showing consecutive collapses and revivals belonging to the $s = 0$ semiclassical and $s = 1, 2$ quantum regimes.

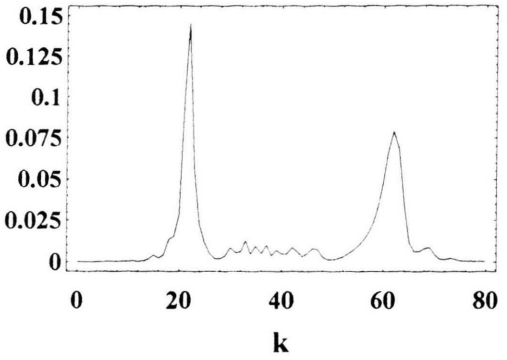

Fig. 13. The photon statistics at $\theta = 943$ exhibit a superposition of two well-separated quantum island states, QIS^+ (high) and QIS^- (low photon number), belonging to the $s = 2$ and $s = 3$ quantum regimes, respectively.

of the oscillations between the well-defined phases, i. e. between QIS^- and QIS^+, as a revival of the phase transitions following the collapse in the semiclassical regime. We should remark here that there are apparent differences in the characteristics of the phase transitions and their collapses between the semiclassical and quantum regimes due to the different origins of the phase structures themselves. The phase transitions between QIS^- and QIS^+ result in the oscillations in the average photon number, $\langle n \rangle$, as depicted in Figs. 8 and 12. Since $\langle n \rangle$ is simply related to the atomic population (see in the Appendix) the same kind of oscillations can be found in the atomic inversion. Therefore, the collapse of the oscillations in the semiclassical region and their revival in the quantum regime are directly connected to the Jaynes-Cummings collapse and revival effect [5]. As we mentioned above there are several consecutive structures in the quantum regime parametrized by $s > 1$ (there is only one in the semiclassical regime, $s = 0$). The disintegration and reshaping of the phase structures, therefore, correspond to a collapse in the semiclassical region and a sequence of consecutive collapses and revivals in the quantum regime, as depicted in Figure 12.

The different regimes of phases can, especially for small N_{ex}, overlap. This usually mixes the phase structures up although, at particular pumping parameters, also allows for a production of (incoherently) superposed QIS corresponding to different regimes. In the example depicted in Fig. 13 the QIS^+ around $k = 62$ belongs to $s = 2$ while QIS^- around $k = 22$ belongs to $s = 3$ resulting in two well-separated coexisting sharp peaks. We have chosen $N_{ex} = 100$ in this paper in order to separate the different structures in the quantum regime for better presentation. However, as it can be easily seen from (3.4), the same phase structures and corresponding QIS arise for lower N_{ex}, as well, at smaller pumping parameters. We, therefore, conclude that the experimental realization of these features of the photon statistics including, in particular, the quantum island states is possible especially for lower values of N_{ex}.

4. Summary

In the present paper, the photon statistics [3] of the micromaser [1] have been studied in the two-dimensional space of the pumping parameter θ and photon number k. We have found that the peaks of the probability distribution form various phase structures in this space transforming into one another as the pumping parameter θ increases. The first group of phases is situated in the so-called "semiclassical" regime determined by the condition given in equation (2.6). The curves of these peaks are monotonous and coincide with the stable steady state solutions of the semiclassical theory [4]. Their structure, together with their populations, i. e. the probability distributions along them, result in typical features in the dynamics of the micromaser, such as the collapsing phase transitions in the average photon number as a function of θ. However, when the pumping θ increases beyond the semiclassical regime, the phases disintegrate due to the discreteness of the photon number. The micromaser enters its "quantum regime". New kinds of phases are formed from the

disintegrated fragments of the old ones that are no longer monotonous. Single large probability peaks, the so-called "quantum island states" (QIS), can arise in the vicinity of their minima that have been absent from the semiclassical regime [8]. In the optimum cases, the system makes periodic phase transitions between the two kinds of quantum island states, QIS^- and QIS^+. These oscillations as a function of θ, together with the collapse of the phase transitions in the semiclassical regime, correspond to the Jaynes-Cummings collapse and revival. The disintegration and transformation of the structure of phases recur periodically as θ increases, and the group of phases in the semiclassical region is followed by a sequence of phase structures in the quantum regime. The mean photon number $\langle n\rangle$ exhibits periodic collapses and revivals corresponding to each structure. Experimental demonstration of these phase structures, including the quantum island states, appears feasible using the presently available facilities.

Acknowledgements

This research was supported by a grant from the Office of Naval Research, grant number N00014-92-J-1233, and by a grant from the PSC-CUNY Research Award Program.

Dedication

It is both an honor and a pleasure to dedicate this paper to Professor Georg Süßmann on the occasion of his 70th birthday. My own view of the world (JB) has been greatly enriched by encounters and conversations with him and by the radiation of his original intellect.

Appendix

Let us consider the master equation of the micromaser for the interaction-picture field density matrix, ρ, given by [8]

$$\frac{\mathrm{d}\rho}{\mathrm{d}t} = r(C\rho C + S^\dagger \rho S) + \mathcal{L}\rho, \tag{A.1}$$

where, in the gain term, $C = \cos(g\tau\sqrt{aa^\dagger})$, $S = [\sin(g\tau\sqrt{aa^\dagger})/\sqrt{aa^\dagger}]a$, and the loss term reads as

$$\mathcal{L}\rho = \frac{\gamma}{2}\Big[(\overline{n}_b + 1)(2a\rho a^\dagger - a^\dagger a\rho - \rho aa^\dagger) + \overline{n}_b(2a^\dagger \rho a - aa^\dagger\rho - \rho aa^\dagger)\Big] \tag{A.2}$$

The equation of motion for the average photon number is [3]

$$\frac{\mathrm{d}}{\mathrm{d}t}\langle n\rangle = r\left\langle \sin^2(g\tau\sqrt{aa^\dagger})\right\rangle - \gamma(\langle n\rangle - \overline{n}_b). \tag{A.3}$$

The same result can be obtained when, assuming separable gain and loss cycles in the case of $\tau \ll 1/\gamma$, we use the return map given by

$$\rho^{(k+1)} = e^{\mathcal{L}/r}(C\rho^{(k)}C + S^\dagger\rho^{(k)}S), \tag{A.4}$$

where k is the number of atoms that have traversed the cavity and $1/r$ is the mean time interval between the atoms for Poissonian pumping statistics. Approximating the time derivative of $\langle n\rangle$ with $r(\langle n\rangle^{(k+1)} - \langle n\rangle^{(k)})$ and assuming $1/r \ll 1/\gamma$, i.e. the cavity lifetime much longer than the time interval between the injection of atoms, we reobtain (A.3). The semiclassical rate equation is found by approximating the quantum expectation values by their semiclassical counterparts as

$$\frac{\mathrm{d}n}{\mathrm{d}t} = r\sin^2(g\tau\sqrt{n+1}) - \gamma(n - \overline{n}_b), \tag{A.5}$$

that results in (2.4) at steady state.

Calculating the atomic density matrix as

$$\rho_{(\mathrm{atom})}(\tau) = \mathrm{Tr}_{(\mathrm{field})}\left[\mathcal{U}(\tau)\rho_{(\mathrm{atom})}(0)\otimes\rho(0)\mathcal{U}^\dagger(\tau)\right] \tag{A.6}$$

where $\mathcal{U}$ is the time evolution operator of the Jaynes-Cummings model, $\rho_{(\mathrm{atom})}(0)$ and $\rho(0)$ are the initial density matrices for the atom and the field, respectively, the matrix element for the lower atomic state is found to be $\rho_{bb} = \langle\sin^2(g\tau\sqrt{aa^\dagger})\rangle$, provided we started with initially excited atoms, $\rho_{aa} = 1$. This can be substituted into (A.3), and we obtain

$$\frac{\mathrm{d}}{\mathrm{d}t}\langle n\rangle = r\rho_{bb} - \gamma(\langle n\rangle - \overline{n}_b). \tag{A.7}$$

Therefore, the steady state average photon number, $\langle n\rangle_{\mathrm{ss}}$, is directly connected to the final atomic population as $\rho_{bb}N_{\mathrm{ex}} = \langle n\rangle_{\mathrm{ss}} - \overline{n}_b$, resulting in the inversion, $w = \rho_{aa} - \rho_{bb}$, given by

$$w = 1 - 2\frac{\langle n\rangle_{\mathrm{ss}} - \overline{n}_b}{N_{\mathrm{ex}}}. \tag{A.8}$$

[1] For a recent review, see H. Walther, Phys. Rep. **219**, 201 (1992); H. Walther, Phys. Scr. **T23**, 165 (1988); F. Diedrich, J. Krause, G. Rempe, M. O. Scully, and H. Walther, IEEE J. Quantum Electron. **QE-24**, 1314 (1988).

[2] E. T. Jaynes and F. W. Cummings, Proc. IEEE **51**, 89 (1963).

[3] The quantum theory of the micromaser is given by P. Filipowicz, J. Javanainen, and P. Meystre, Phys. Rev. A **34**, 3077 (1986); L. A. Lugiato, M. O. Scully, and H. Walther, Phys. Rev. A **36**, 740 (1987).

[4] For the semiclassical theory see A. M. Guzman, P. Meystre, and E. W. Wright, Phys. Rev. A **40**, 2471 (1989).

[5] H. Paul, Ann. Phys. (Leipzig) **11**, 411 (1963); J. H. Eberly, N. B. Narozhny, J. J. and Sanchez-Mondragon, Phys. Rev. Lett. **23**, 44 (1980). The experimental proof of the quantum collapse and revival predicted by the Jaynes-Cummings model was reported by G. Rempe, H. Walther, and N. Klein, Phys. Rev. Lett. **58**, 353 (1987).

[6] J. Krause, M. O. Scully, and H. Walther, Phys. Rev. A **36**, 4547 (1987); P. Meystre, Opt. Lett. **12**, 668 (1987); H. Paul, J. Mod. Opt. **36**, 515 (1989); F. W. Cummings and A. K. Rajagopal, Phys. Rev. A **39**, 3414 (1989).

[7] P. Meystre, G. Rempe, and H. Walther, Opt. Lett. **13**, 1078 (1988).

[8] P. Bogár, J. A. Bergou, and M. Hillery, Phys. Rev. A **50**, 754 (1994).

[9] P. Filipowicz, J. Javanainen, and P. Meystre, J. Opt. Soc. Amer. B **3**, 906 (1986); J. J. Slosser, P. Meystre, and S. L. Braunstein, Phys. Rev. Lett. **63**, 934 (1989); J. J. Slosser and P. Meystre, Phys. Rev. A **41**, 3867 (1990); J. J. Slosser, P. Meystre, and E. M. Wright, Opt. Lett. **15**, 233 (1990); P. Meystre, J. J. Slosser, and M. Wilkens, Phys. Rev. A **43**, 4959 (1991).

[10] L. Davidovich, A. Maali, M. Brune, J. M. Raimond, and S. Haroche, Phys. Rev. Lett. **71**, 2360 (1993); J. A. Bergou and M. Hillery, Phys. Rev. A **44**, 7502 (1991); P. Bogár, J. A. Bergou, and M. Hillery, Phys. Rev. A **51**, 2396 (1995); P. Bogár and J. A. Bergou, Phys. Rev. A **51**, 2381 (1995); J. A. Bergou, M. Hillery, and P. Bogár, Phys. Rev A. submitted (1998).

[11] M. O. Scully and H. Walther, Phys. Rev. A **39**, 5229 (1989); M. O. Scully, B.-G. Englert, and H. Walther, Nature London **351**, 111 (1991); B.-G. Englert, H. Walther, and M. O. Scully, Appl. Phys. B **54**, 366 (1992); P. Bogár and J. A. Bergou, Phys. Rev. A **53**, 49 (1996).